Published in final edited form as:
*Ann Biomed Eng*. 2010 December ; 38(12): 3605–3617. doi:10.1007/s10439-010-0114-3.

# Biomechanical and Microstructural Properties of Common Carotid Arteries from Fibulin-5 Null Mice

**William Wan**[1], **Hiromi Yanagisawa**[4], and **Rudolph L. Gleason Jr.**[1,2,3]

[1] The George W. Woodruff School of Mechanical Engineering, Georgia Institute of Technology, 801 Ferst Drive, Atlanta, GA 30332, USA

[2] The Wallace H. Coulter Department of Biomedical Engineering, Georgia Institute of Technology, 313 Ferst Drive, Atlanta, GA 30332, USA

[3] The Petite Institute for Bioengineering and Bioscience, Georgia Institute of Technology, 315 Ferst Drive, Atlanta, GA 30332, USA

[4] The University of Texas Southwestern Medical Center, 6000 Harry Hines Blvd. NA5.320, Dallas, TX 75390, USA

## Abstract

Alteration in the mechanical properties of arteries occurs with aging and disease, and arterial stiffening is a key risk factor for subsequent cardiovascular events. Arterial stiffening is associated with the loss of functional elastic fibers and increased collagen content in the wall of large arteries. Arterial mechanical properties are controlled largely by the turnover and reorganization of key structural proteins and cells, a process termed growth and remodeling. Fibulin-5 (*fbln5*) is a microfibrillar protein that binds tropoelastin, interacts with integrins, and localizes to elastin fibers; tropoelastin and microfibrillar proteins constitute functional elastic fibers. We performed biaxial mechanical testing and confocal imaging of common carotid arteries (CCAs) from fibulin-5 null mice ($fbln5^{-/-}$) and littermate controls ($fbln5^{+/+}$) to characterize the mechanical behavior and microstructural content of these arteries; mechanical testing data were fit to a four-fiber family constitutive model. We found that CCAs from $fbln5^{-/-}$ mice exhibited lower *in vivo* axial stretch and lower *in vivo* stresses while maintaining a similar compliance over physiological pressures compared to littermate controls. Specifically, for $fbln5^{-/-}$ the axial stretch $\lambda = 1.41 \pm 0.07$, the circumferential stress $\sigma_\theta = 101 \pm 32$ kPa, and the axial stress $\sigma_z = 74 \pm 28$ kPa; for $fbln5^{+/+}$ $\lambda = 1.64 \pm 0.03$, $\sigma_\theta = 194 \pm 38$ kPa, and $\sigma_z = 159 \pm 29$ kPa. Structurally, CCAs from $fbln5^{-/-}$ mice lack distinct functional elastic fibers defined by the lamellar structure of alternating layers of smooth muscle cells and elastin sheets. These data suggest that structural differences in $fbln5^{-/-}$ arteries correlate with significant differences in mechanical properties. Despite these significant differences $fbln5^{-/-}$ CCAs exhibited nearly normal levels of cyclic strain over the cardiac cycle.

### Keywords

Vascular mechanics; Extracellular matrix; Arterial stiffening; Mechanobiology; Fibulin-5



Address correspondence to Rudolph L. Gleason Jr., The George W. Woodruff School of Mechanical Engineering, Georgia Institute of Technology, 801 Ferst Drive, Atlanta, GA 30332, USA. rudy.gleason@me.gatech.edu.

## INTRODUCTION

Alteration in the mechanical properties of arteries occurs with aging and disease, and arterial stiffening is an independent predictor of cardiovascular risk.[1] Arterial stiffening is associated with the loss of functional elastic fibers and increased collagen content in the wall of large arteries. It is clear that vascular endothelial cells, smooth muscle cells, and fibroblasts demonstrate the remarkable ability to respond to mechanical stimuli via mechanotransduction mechanisms and to control the material properties and local mechanical environment in the arterial wall. This process occurs largely via delicate balances (or imbalances) in the synthesis, degradation, and reorganization of structural proteins and cells,[4,7] a process termed growth and remodeling.[16] Genetically-modified animal models provide a unique opportunity to alter the content and organization of key microstructural proteins. [8,30] Such models provide a platform to quantify the role of key structural proteins on the mechanical properties of arteries.

Fibulin-5, also known as DANCE (*d*evelopmental *a*rteries and *n*eural *c*rest *E*GF-like) or EVEC (*e*mbryonic *v*ascular *E*GF-like repeat-*c*ontaining protein), is an extracellular matrix protein that is essential for elastic fiber formation and is expressed in developing arteries as well as balloon-injured and atherosclerotic arteries.[21] *fbln5* localizes to elastic fibers and binds to tropoelastin and interacts with various integrins, including $\alpha_V\beta_3$.[20] Mice lacking both alleles of the *fbln5* gene experience loose skin, emphysema, tortuous blood vessels, and increased arterial stiffness.[24,32] Although adequate tropoelastin is present in large arteries of *fbln5* knockout mice, this tropoelastin was not organized into functional elastic lamina in these vessels.[32] Given these coincident microstructural and mechanical differences, $fbln5^{-/-}$ mice provide a good model to study the effect of altered functional elastic fibers on the mechanical behavior of elastic arteries.

The purpose of this study is to quantify the biaxial biomechanical response and to qualitatively evaluate the microstructural content and organization of mouse common carotid arteries (CCAs) from $fbln5^{-/-}$ mice and littermate controls. We performed biaxial mechanical tests and performed multiphoton (confocal) microscopy imaging on isolated carotid artery segments from $fbln5^{+/+}$ and $fbln5^{-/-}$ mice. Biaxial tests revealed that arteries from $fbln5^{-/-}$ mice were circumferentially and axially stiffer with a lower *in vivo* axial stretch than arteries from $fbln5^{+/+}$ mice. Confocal microscopy images showed that, in contrast to $fbln5^{+/+}$ CCAs, $fbln5^{-/-}$ CCAs lacked organized elastic lamellae and that collagen fibers in $fbln5^{-/-}$ CCAs engage at lower axial stretch ratios. Although vascular stiffness was elevated in $fbln5^{-/-}$ vessels, since the *in vivo* pulse pressure is also higher in $fbln5^{-/-}$ vessels, the cyclic strains in $fbln5^{-/-}$ and $fbln5^{+/+}$ CCAs were not statistically different.

## METHODS

### Surgical Preparation and Vessel Isolation

Adult male mice, $fbln5^{-/-}$ (13 ± 5 weeks old, $n = 6$) and $fbln5^{+/+}$ (13 ± 1 weeks old, $n = 7$) littermate controls on the C57BL/6 × 129/SvEv background were anesthetized with sodium pentobarbital (100 mg/kg IP). All mice were produced from a breeding pair originally obtained from Dr. Hiromi Yanagisawa (UT Southwestern). Under sterile conditions, both CCAs were excised, placed in fresh culture medium, dissected free of perivascular tissue, and mounted on the glass cannulae of our biomechanical testing device using sterile suture.[11] All animal procedures were approved by the Institute Animal Care and Use Committee (IACUC) at the Georgia Institute of Technology.

## Biomechanical Testing

A device modified from one reported by Gleason *et al.*[11] was used to perform cylindrical biaxial biomechanical and vasoreactivity tests and to perform multi-photon, confocal microscopy. Pressure–diameter (*P–d*) data were collected from 0 to 180 mmHg at constant axial extensions, and axial force–length (*f*–ℓ) data were collected over cyclic axial extensions up to $\lambda = 1.70$ for $fbln5^{+/+}$ arteries and $\lambda = 1.55$ for $fbln5^{-/-}$ arteries at constant pressures, $P = 60$, 100, and 160 mmHg. Here, $\lambda = \ell/L$ where ℓ is the current length and $L$ is the original unloaded length; ℓ and $L$ were measured as the distance between mounting sutures. The *in vivo* axial stretch ratio was defined as the stretch for which axial force remains nearly constant during the pressurization cycle.[5,27]

*P–d* tests were performed at stretches above and below the *in vivo* axial stretch ratio and were performed at different sets of axial extensions for $fbln5^{-/-}$ and $fbln5^{+/+}$ arteries. All *P–d* and *f*–ℓ tests were performed quasi-statically over 3 loading–unloading cycles, and to prevent damage from over stretching, the maximum axial load was limited to 9 and 4.4 mN for $fbln5^{+/+}$ and $fbln5^{-/-}$ vessels, respectively. Tests were performed in the same order for all vessels; *P–d* at $\lambda <$ *in vivo* axial stretch, *P–d* at $\lambda \sim$ *in vivo* axial stretch, *P–d* at $\lambda >$ *in vivo* axial stretch, *f*–ℓ at $P = 60$ mmHg, *f*–ℓ at $P = 100$ mmHg, and *f*–ℓ at $P = 160$ mmHg. Vessel wall thickness was measured using a custom videocaliper LabView subroutine by measuring the inner and outer diameter of the vessel following Gleason *et al.*[11]

Immediately following these ('basal') biomechanical tests, vessels were loaded to $P = 90$ mmHg and $\lambda =$ *in vivo* axial stretch ratio, and allowed to stabilize for 15 min. Contractile function was then assessed by measuring relative changes in diameter and axial force in response to the sequential administration vasoactive agents to the bathing media: phenylephrine (PE) or norepinephrine (NE) to elicit smooth muscle cell contraction, carbamylcholine chloride (CCh) to elicit endothelial-dependent dilation, and sodium nitroprusside (SNP) to elicit endothelial-independent dilation.[11] Values of diameter and axial force were normalized to values measured at the end of the 15-min recovery period.

## Opening Angle

It is well known that the traction-free configuration of arteries is typically not stress-free; rather these unloaded vessels contain residual stresses.[3] To quantify the degree of residual stress in these arteries, opening angle measurements were made. Multiple unloaded rings were cut from excised carotid arteries (17 $fbln5^{-/-}$ and 12 $fbln5^{+/+}$ total), and a single radial cut was imposed, which caused the vessel rings to spring open, relieving much of the residual stress. The opening angle, $\Phi_o$, was calculated as

$$\Phi_o = \pi - \frac{L_o - L_i}{2H} \quad \text{and} \quad A = \frac{H(L_o + L_i)}{2} \tag{1}$$

where the second term on the right-hand side of Eq. $(1)_1$ is the half-angle of the open sector as defined by Chuong and Fung,[3] $L_o$ and $L_i$ are the outer and inner arc lengths of the stress-free sector, $H$ is the wall thickness of the stress-free sector and $A$ is the cross-sectional area of the wall in the open sector. A mean value for $H$ was calculated by measuring the area of the sector and using Eq. $(1)_2$.

## Stress, Strain, and Compliance

The mean circumferential stress ($\sigma_\theta$) and axial stress ($\sigma_z$) were then calculated as

$$\sigma_\theta = \frac{Pa}{h} \quad \text{and} \quad \sigma_z = \frac{f}{\pi(b^2 - a^2)} \tag{2}$$

where $P$ is the transmural pressure, $a$ is the current inner radius, $b$ is the current outer radius, $h$ is the current thickness, and $f = f_m + \pi a^2 P$ is the force applied to the vessel wall; $f_m$ is the force measured by the force transducer. The mean circumferential and axial components of the Green Strain were calculated as

$$\overline{E}_{\theta\theta} = \frac{\overline{\lambda}_\theta^2 - 1}{2} \quad \text{and} \quad \overline{E}_{zz} = \frac{\overline{\lambda}^2 - 1}{2} \tag{3}$$

where the mean circumferential stretch was calculated as $\bar{\lambda}_\theta = r_{mid}/\rho_{mid}$, using mid-wall loaded and unloaded radii $r_{mid} = (a + b)/2$ and $\rho_{mid} = (\rho_o - \rho_i)/2$, respectively; here $\rho_i$ and $\rho_o$ are the unloaded inner and outer radii. Compliance is defined through the relation

$$C\Delta P = \Delta\varepsilon = \frac{\Delta r_m}{\bar{r}_m} \tag{4}$$

where $C$ is compliance, $\Delta r_m$ is the difference in the mid-wall radii measurements at two different pressures, $\bar{r}_m$ is the mid-wall radius at the mean pressure, $\Delta P$ is difference in the two pressures, and $\Delta\varepsilon$ is the local linearized cyclic strain experienced over $\Delta P$. Physiological blood pressures were defined as 133/92 mmHg (systole/diastole) for *fbln5*$^{+/+}$ mice and 151/94 mmHg for *fbln5*$^{-/-}$ mice.[32]

## Statistical Analysis

Mean values were compared using unpaired, two-tailed *t*-tests, with significance taken at $p<0.05$. Welch's correction was used when variances between groups were unequal.

## Multiphoton Microscopy

Freshly isolated vessels were imaged on an LSM 510 META inverted confocal microscope (Zeiss). The laser reached the sample through either a 40×/1.3NA or a 63×/1.4NAoil immersion objective (Zeiss). The META module of the microscope was configured as a 380–420-nm bandpass filter to detect backward scattering second-harmonic generation (SHG) signal from collagen.[33] Elastin was detected using a 500–550-nm bandpass filter with 488 nm laser excitation.[31] Confocal microscopy of embedded sections showed nearly identical morphology of elastin and collagen as samples stained with Verhoeff's and picro sirius red stains. Smooth muscle cells were visualized by staining the extracellular space with carboxyfluorescein.[22] Imaris software (Bitplane) was used for 3D reconstruction of images.

## Constitutive Modeling

**Kinematics—**We considered three configurations: a loaded configuration $\beta_t$, a traction-free (unloaded) configuration $\beta_u$, and a (nearly stress-free) reference configuration $\beta_o$; see Chuong and Fung.[3] For inflation and extension of an axisymmetric tube, the deformation gradient, right Cauchy Green strain, and Green strain tensors have components

$$[\mathbf{F}]=\mathrm{diag}\{\lambda_r,\lambda_\theta,\lambda_z\},\quad [\mathbf{C}]=\mathrm{diag}\{\lambda_r^2,\lambda_\theta^2,\lambda_z^2\},$$
$$[\mathbf{E}]=\mathrm{diag}\{(\lambda_r^2-1)/2,(\lambda_\theta^2-1)/2,(\lambda_z^2-1)/2\} \tag{5}$$

where

$$\lambda_r=\frac{\partial r}{\partial R},\quad \lambda_\theta=\frac{\pi r}{\Theta_o R}\quad \text{and}\quad \lambda_z=\lambda\Lambda, \tag{6}$$

and $\Lambda$ and $\lambda$ are the axial stretches for the motions from $\beta_o$ to $\beta_u$ and from $\beta_u$ to $\beta_t$, respectively, and $\Theta_o = (\pi - \Phi_o)$ is the sector angle in $\beta_o$. If the material is assumed to be incompressible, $\det(\mathbf{F}) = 1$, the current radius may be related to the reference radius (in $\beta_o$) as

$$r=\sqrt{\frac{\Theta_o}{\pi\lambda\Lambda}(R^2-R_i^2)+r_i^2}\ \text{ or }\ r=\sqrt{r_o^2-\frac{\Theta_o}{\pi\lambda\Lambda}(R_o^2-R^2)}, \tag{7}$$

where $R_i$ and $R_o$ are inner radii or outer radii in $\beta_o$ and $r_i$ and $r_o$ are inner and outer radii in $\beta_t$. Thus, given measured values for the reference configuration ($R_i$, $R_o$, the unloaded axial length $L_z$, and $\Theta_o$) and the current configuration ($r_o$, $r_i$, and the loaded length $\ell$), the components of **F**, **C**, and **E** are easily calculated.

**Equilibrium—**Inflation and extension of a long, straight, axisymmetric, closed-ended tube in equilibrium requires that

$$P=\int_{r_i}^{r_o}(\widehat{T}_{\theta\theta}-\widehat{T}_{rr})\frac{dr}{r}\ \text{ and}$$
$$f_m=\pi\int_{r_i}^{r_o}(2\widehat{T}_{zz}-\widehat{T}_{\theta\theta}-\widehat{T}_{rr})r\,dr; \tag{8}$$

where

$$\mathbf{T}=\widehat{\mathbf{T}}-p\mathbf{I}\quad \text{where}\quad \widehat{\mathbf{T}}=2\mathbf{F}(\partial W/\partial\mathbf{C})\mathbf{F}^{\mathrm{T}} \tag{9}$$

$\hat{\mathbf{T}}$ is the so-called ‘extra’ stress due to the deformation, and $W$ is the strain energy density function; see Humphrey.[15]

**Constitutive Equation—**We used a four fiber-family model proposed by Baek *et al.*[2] which is a simple extension of the model proposed by Holzapfel *et al.*[13] and Spencer,[26] with strain energy function

$$W=\frac{b}{2}(I_1-3)+\sum_{k=1,2,3,4}\frac{b_1^k}{2b_2^k}\left\{\exp\left[b_2^k\left((\lambda^k)^2-1\right)^2\right]-1\right\} \tag{10}$$

where $b$, $b_1^k$, and $b_2^k$ are material parameters with $k$ denoting a fiber family, $I_1 = \mathrm{tr}(\mathbf{C}) = C_{rr} + C_{\theta\theta} + C_{zz}$ is the first invariant of $\mathbf{C}$, $\lambda^k = \sqrt{\mathbf{M}^k \cdot \mathbf{C}\mathbf{M}^k}$ is the stretch of the $k$th fiber family, $\mathbf{M}^k = \sin(\alpha^k)\mathbf{e}_\theta + \cos(\alpha^k)\mathbf{e}_z$ is the unit vector along the $k$th fiber direction in the reference configuration, and $\alpha^k$ is the associated angle between the axial and fiber directions. In general, $(\lambda^k)^2 = C_{\theta\theta}\sin^2(\alpha^k) + 2C_{\theta z}\sin(\alpha^k)\cos(\alpha^k) + C_{zz}\cos^2(\alpha^k)$, but $C_{\theta z} = 0$ for inflation and extension tests, given material symmetry. Under compression, the fiber families do not contribute to the mechanical response in an exponential fashion, as they do in tension. Thus, when $\lambda^k<1$, we set $b_1^k=0$; therefore, we model the vessel under compression as a neo-Hookean material. Here, we consider four-fiber families with $\alpha^1 = 90°$ (circumferential), $\alpha^2 = 0°$ (axial), and $\alpha^3 = -\alpha^4 = \alpha$ (diagonal) which is left as a variable to be determined along with the seven material parameters (with $b_1^3=b_1^4$ and $b_2^3=b_2^4$ for the diagonal fibers to ensure material symmetry) via non-linear regression.

**Parameter Estimation—**Equations $(8)_1$ and $(8)_2$ were used to calculate $P$ and $f$ based on measured values of outer diameter, axial length, unloaded radius, unloaded length and wall thickness. We employ Eq. (6), with Eq. (7), and specify the *in vivo* configuration and transmural strains in this configuration to determine $\mathbf{F}$ and $\mathbf{C}$. Material parameters were identified via nonlinear regression by minimizing the error function

$$\mathrm{Error}=\left\{\sum_{i=1}^{N}\left(\frac{P_{\mathrm{meas}}(i)-P_{\mathrm{model}}(i)}{\bar{P}}\right)^2+\sum_{i=1}^{N}\left(\frac{f_{\mathrm{meas}}(i)-f_{\mathrm{model}}(i)}{\bar{f}}\right)\right\}^2 \tag{11}$$

where $P_{\mathrm{meas}}(i)$ and $f_{\mathrm{meas}}(i)$ are measured values and $P_{\mathrm{model}}(i)$ and $f_{\mathrm{model}}(i)$ are predicted values of pressure and axial force for data point $i$ and $\bar{P}$ and $\bar{f}$ are mean values of pressure and force over all data points. Thus, Eq. (11) quantifies the difference between experimental data and modeling predictions. Calculations were performed in MatLab 7.1 using the *lsqnonlin* subroutine.

## RESULTS

### Mechanical Response of fbln5$^{-/-}$ Arteries and Controls

Pressure–diameter tests of *fbln5*$^{+/+}$ mice and *fbln5*$^{-/-}$ mice revealed distinct regimes over lower pressure and higher pressure ranges characteristic of rodent large arteries (Fig. 1a). Not all curves reached 180 mmHg because tests were stopped when the axial force reached the maximum limit or when the axial force became negative. Force measurements taken during *P–d* tests indicated that at lower axial stretch ratios, axial force decreases with increased pressure while at higher axial stretch ratios, axial force increases with increased pressure (Fig. 1b). Although the range of axial stretch ratios used for testing was different for the *fbln5*$^{-/-}$ and *fbln5*$^{+/+}$ groups, there were stretch ratios that overlapped both groups. Namely, at $\lambda = 1.40$, it is clear that the mechanical responses of the two types of vessels are different (Fig. 1b). For each vessel tested, there was an axial stretch ratio for which the force remains nearly constant with increased pressure, indicating the *in vivo* axial stretch ratio.[5,27] Mid-wall radii were calculated at the *in vivo* axial stretch ratio revealing significant

differences in geometry at pressures greater than or equal to 70 mmHg (Fig. 2a and Table 1). In addition, the axial force was significantly different between groups when measured at the *in vivo* axial stretch ratio (Fig. 2b). Given the significantly lower *in vivo* axial stretch of the *fbln5*$^{-/-}$ vessels, *P–d* tests for *fbln5*$^{-/-}$ vessels were performed at lower axial stretch ratios than *fbln5*$^{+/+}$ vessels. Results from axial force–length tests (Fig. 3) revealed a cross-over point which represents the *in vivo* axial stretch ratio[28]; the mean *in vivo* axial stretch ratio of *fbln5*$^{-/-}$ arteries was $\lambda = 1.41$, compared to a mean *in vivo* axial stretch ratio of $\lambda = 1.64$ in *fbln5*$^{+/+}$ arteries (Table 1). The *in vivo* axial stretch ratios as determined from *f*–ℓ tests were similar to the axial stretch ratio determined from *P–d* tests.

## Stress, Strain, and Compliance

Since the pressure–diameter and axial force–length responses depend on both material properties and geometry, it is difficult to quantify differences in the material properties between different vessels from *P–d* and *f*–ℓ plots. Stress–strain plots, however, only depend on material properties; thus, differences in the stress–strain response indicate differences in the material properties. While large segments of the mean stress–strain plots in both circumferential and axial directions overlap (Fig. 4), calculations based on *in vivo* axial stretch and mean blood pressures reveal significant differences in both *in vivo* axial and circumferential stresses (Table 1). Mean circumferential and axial (Cauchy) stress vs. mid-wall Green strain reveal significant differences in the material response between *fbln5*$^{+/+}$ and *fbln5*$^{-/-}$ vessels (Figs. 4a and 4b). In other words, the exponentially stiffening portion of the stress strain plots occurs at lower strains for *fbln5*$^{-/-}$ vessels. The overall compliance, between systolic and diastolic pressures, of the *fbln5*$^{-/-}$ CCAs was not statistically different than *fbln5*$^{+/+}$ CCAs. The *in vivo* local linearized cyclic strain $\Delta\varepsilon$ over the cardiac cycle was also not statistically different across groups (Table 1). The local compliance, calculated at 10 mmHg intervals, was also not significantly different at the overlapping physiological pressures; however, compliance was different at 50, 60, 70, 80, and 150 mmHg (Fig. 5).

## Stress-Free, Unloaded, and Loaded Configuration

Excised *fbln5*$^{+/+}$ carotid arteries exhibited slight bending upon excision compared to the marked tortuosity of *fbln5*$^{-/-}$ arteries (Fig. 6). Opening angles of sectors cut from *fbln5*$^{-/-}$ arteries were statistically greater than angles of *fbln5*$^{+/+}$ arteries (Fig. 7 and Table 1), and there was also greater variability across samples in opening angle measurements from *fbln5*$^{-/-}$ arteries. Inner diameter, outer diameter, and wall thickness were not statistically different in unloaded, traction-free configurations of *fbln5*$^{+/+}$ and *fbln5*$^{-/-}$ arteries. Under physiological loading conditions, *fbln5*$^{-/-}$ vessels had significantly smaller inner and outer diameters and larger wall thicknesses than the *fbln5*$^{+/+}$ vessels (Table 1).

## Functional Response

Following ‘basal’ biomechanical testing, smooth muscle and endothelial cell function was confirmed by pharmacologically induced constriction and dilation. Both *fbln5*$^{-/-}$ and *fbln5*$^{+/+}$ vessels decreased in diameter in response vasoconstrictors while relaxing to near basal levels of outer diameter in response to vasodilators (Table 1). Both wild-type and knockout vessels exhibited significant differences in normalized diameter at maximal contraction and normalized diameter at maximal relaxation.

## Microstructural Organization

In the traction-free configuration, elastin from the *fbln5*$^{+/+}$ artery appeared undulated with a distinct internal elastic lamina while elastin in the *fbln5*$^{-/-}$ artery appears disorganized with no distinct internal lamina (Fig. 8). Under *in vivo* conditions, distinct layers of elastin are visible in the *fbln5*$^{+/+}$ artery while the *fbln5*$^{-/-}$ artery lacks noticeable lamellar units (Fig. 8).

Collagen in the traction-free configuration appears to exist with varying degrees of undulation in the *fbln5*$^{-/-}$ and the *fbln5*$^{+/+}$ arteries (Fig. 9). Under identical conditions of axial stretch and transmural pressure, collagen fibers in *fbln5*$^{-/-}$ arteries appear to be straightened and engaged while collagen fibers in *fbln5*$^{+/+}$ arteries appear undulated (Fig. 9). Under *in vivo* conditions, individual smooth muscle cells show similar morphology in both *fbln5*$^{-/-}$ and the *fbln5*$^{+/+}$ arteries; however, distinct lamellar units were visible in the *fbln5*$^{+/+}$ arteries (Fig. 10).

### Parameter Estimation

A four-fiber model was able to capture the full range of mechanical behaviors in both *fbln5*$^{-/-}$ and the *fbln5*$^{+/+}$ arteries (Fig. 11). The lower and upper limits of the parameters were prescribed as $b$ and $b_1^k \in [0, 10^5]$, $b_2^k \in [10^{-4}, 10^5]$, and $\alpha \in [0°, 90°]$. The upper bounds were selected to encompass the full working range of individual parameters, and the non-zero lower bound for $b_2^k$ was selected to prevent the algorithm from searching for values close to zero. Final parameter values were insensitive to initial guesses. The mean values of Error = 0.058 and Error = 0.042 indicate reasonably good fits to experimental data; error values on (Table 2) reflect the error calculated from Eq. (11) normalized to the total number of data points for each vessel. A significant increase in $b_2^2$ and $b_2^3$ was seen for the *fbln5*$^{-/-}$ groups (Table 2); these are the parameters in the exponential terms for the axially and diagonally oriented fiber families Eq. (10). Note that the elastic modulus term, $b$, was lower in *fbln5*$^{-/-}$ vessels; however, this difference was not statistically significant.

## DISCUSSION

Since the classic article by Roach and Burton, it is thought that functional elastic fibers in large arteries mediate the shape of the pressure–diameter curves at low pressures while collagen mediates this behavior at higher pressures.[25] Genetically altered mouse models that suppress expression of tropoelastin and microfibrillar proteins (e.g., fibrillins and fibulins) provide a unique platform to study the role of functional elastic fibers in the mechanical response of arteries.[8,30] In this study, we quantified the mechanical properties of *fbln5*$^{-/-}$ CCAs, which lack functional elastic laminae, and the *fbln5*$^{+/+}$ arteries, which have normal elastic laminae. We performed biaxial mechanical tests and multiphoton (confocal) microscopy imaging on isolated carotid artery segments from *fbln5*$^{+/+}$ and *fbln5*$^{-/-}$ mice. Biaxial tests revealed that arteries from *fbln5*$^{-/-}$ mice were circumferentially and axially stiffer with a lower *in vivo* axial stretch ratio than arteries from *fbln5*$^{+/+}$ mice. Although vascular stiffness was elevated in *fbln5*$^{-/-}$ vessels, since the *in vivo* pulse pressure is also higher in *fbln5*$^{-/-}$ vessels, the cyclic strains in *fbln5*$^{-/-}$ and *fbln5*$^{+/+}$ CCAs were not statistically different. This result suggests that, although significant microstructural differences exist between *fbln5*$^{-/-}$ and *fbln5*$^{+/+}$ CCAs, growth and remodeling mechanisms that occur throughout development have altered the geometry and microstructural organization to achieve similar values of cyclic strain. Confocal microscopy images reveal significant differences in the structure of elastin and the organization of smooth muscle cells of *fbln5*$^{-/-}$ CCAs. In contrast to *fbln5*$^{+/+}$ CCAs, *fbln5*$^{-/-}$ CCAs lacked organized elastic lamellae and had collagen fibers that engaged in load bearing at lower axial stretch ratios. These differences in microstructure were coincident with elevated vascular stiffness and a lower *in vivo* axial stretch ratio in *fbln5*$^{-/-}$ vessels. Constitutive modeling revealed that the mechanical behavior of *fbln5*$^{+/+}$ and *fbln5*$^{-/-}$ vessels could be described well with the four-fiber family model of Baek *et al.*[2]

These microstructural differences manifest in significant differences in the biaxial biomechanical behavior across these groups. In particular, loss of functional elastic laminae

results in vessels with an 15% reduction in *in vivo* mid-wall diameter, a 75% increase *in vivo* wall thickness, a 15% reduction in *in vivo* axial stretch, and a ~50% reduction in *in vivo* stresses. It appears that the presence of functional elastic laminae in control vessels serve to increase the *in vivo* axial stretch ratio and prevent vessel tortuosity. In $fbln5^{-/-}$ arteries, the exponential stiffening region of the stress–strain plot occurs at lower axial and circumferential strains. This phenomenon can be further illustrated by images of collagen from knockout and wildtype arteries that are pressurized and stretched to identical loading conditions. Collagen fibers seen in $fbln5^{-/-}$ CCAs at an axial stretch of $\lambda = 1.4$ and pressure of $P = 40$ mmHg appear straightened while collagen fibers from $fbln5^{+/+}$ arteries remain undulated (Fig. 9).

Decreases in *in vivo* axial stretch have been observed in mice deficient in elastin (*eln*), fibrillin-1 (*fbn1*), dystrophin (mdx), and sarcoglycan-$\delta$ (sgcd).[6,8,30] In addition to a lower *in vivo* axial stretch ratio and reduced elastin content, CCAs of elastin haploinsufficient mice also exhibit arterial tortuosity, and lower outer diameters. Despite these differences, and in contrast to our $fbln5^{-/-}$ data, there were no significant differences in circumferential and axial stress-stretch relationships when held near the *in vivo* stretch and no differences in opening angles between the elastin haploinsufficient and control CCAs or abdominal aorta.[30] For a mouse model of Marfan's Syndrome in which fibrillin-1 is reduced to 15–25% of normal levels ($fbn1^{R/R}$), CCAs exhibit similar *in vivo* outer diameters, but 5% reduction in *in vivo* axial stretches compared to control vessels; namely, the axial stretch in $fbn1^{R/R}$ was $1.63 \pm 0.02$, compared to $1.71 \pm 0.02$ in wildtype controls. Again, in contrast to our data, there are no significant differences in the circumferential mechanical behavior at *in vivo* axial stretches between the $fbn1^{R/R}$ and control CCAs. Force length tests, however, suggest differences in axial stress between $fbn1^{R/R}$ arteries and wild-type controls at pressures from $P = 60$ mmHg to $P = 100$ mmHg and at axial stretches above $\lambda = 1.64$. In mouse models of muscular dystrophy pressure–diameter relationships near the *in vivo* axial stretch ratio are not statistically different.[6] Thus, it appears that the presence of some functional elastic fibers, even in lowered quantities, is sufficient to allow large arteries to adapt to achieve normal circumferential *in vivo* mechanical behavior. Arterial tortuosity was also not noted in studies of mice deficient in *fbln1*, *mdx* and *sgcd* suggesting that the decrease in the production of functional elastic fibers is the cause of tortuosity.[6,8] Biomechanical properties of elastin knockout mice ($Eln^{-/-}$) show significant geometric and mechanical differences; however, these mice die within 72 h of birth.[29] Our study, as well as others, highlights the need to further investigate the axial mechanical behavior of arteries.

To quantify the local mechanobiological response of cells to their local mechanical environment, it is necessary to accurately predict their local mechanical environment; this requires a constitutive model with adequate predictive capability. Given that growth and remodeling are controlled through turnover and remodeling of key structural constituents, we submit that such a constitutive model should be structurally motivated; thus, we employed a fiber family model. Parameter estimation results suggest significant differences in the material properties of $fbln5^{-/-}$ arteries. Each artery was modeled as anisotropic axial, circumferential and diagonal fibers embedded in an isotropic matrix. The isotropic portion of the vessel is associated with the parameter, $b$, while the anisotropic fibers are associated with $b_1^k$ and $b_2^k$. Parameter estimation studies indicated increases in exponential terms, $b_2^2$ and $b_2^3$, for $fbln5^{-/-}$ arteries. These two parameters suggest differences in the mechanical behavior of axial and diagonal portions of the model. Because this constitutive relation does not account for mass fractions and altered crosslinking of constituents, differences in the structural configuration of constituents could have produced the changes observed in these parameters. A few parameters were zero highlighting the relative degree of exponential behavior of that fiber family. A fiber family with a $b_2^k$ term near zero or very much smaller

than the $b_1^k$ term would exhibit high degree of exponentially stiffening behavior. There was also a large degree in variability in some of the parameters such as the case of $b$ for *fbln5*$^{-/-}$ mice and $b_1^2$ for both groups. Large variations in parameters describing experiments that exhibit similar mechanical behaviors highlights the sensitivity of parameters to small perturbations in biaxial test data and is characteristic of constitutive relations with exponential terms.[10,14] Results from parameter estimation studies illustrate the need for detailed investigation of the structure of arteries as well the need for constitutive relations that account for the structural components of the arterial wall.[12]

Mechanically induced vascular remodeling occurs as cells sense and adapt their local mechanical environment and plays a key role in many physiological and pathophysiological processes, as well as in the outcomes of many clinical interventions; examples include arterial stiffening with age, development of aneurysms, hypertension, atherosclerosis, and restenosis of vascular grafts. These adaptations (or maladaptations) are controlled largely by delicate balances (or imbalances) in the production, removal, and reorganization of structural proteins.

Whereas much attention has been paid to the role of wall shear stress and circumferential (hoop) stress in vascular remodeling and cardiovascular disease, the role of axial stress has been largely overlooked. Findings suggest, however, that altered axial stretch (or stress) induces remodeling at rates that are ‘unprecedented’ compared to that of pressure and flow.[18] We submit that cells sense and respond to their local mechanical environment and grow and remodel to restore their local mechanical environment to a ‘desired’ state. Many clinical observations highlight the importance of axial remodeling in the vasculature; marked tortuosity in abdominal aortic aneurysms (AAAs), mammary artery by-pass grafts, and reduced axial strain in hypertension and aging are but a few examples. Circumferential expansion, wall thinning and axial lengthening of AAAs is coincident with a progressive loss of elastin and smooth muscle and a decrease in glycosaminoglycans. Indeed, the level of aortic tortuosity is among the greatest indicators of risk for AAA rupture.[9] These observations suggest that elastic fibers endow arteries with their *in vivo* axial strain, and the loss of functional elastic fibers (which occurs in AAAs, hypertension, and aging) may be associated with impaired axial remodeling and development of tortuosity.

The lack of differences in compliance at pressures within the physiological range as well as differences in physiological geometry suggests that compliance (or cyclic strain) may be a primary target for adaptations in vascular growth and remodeling. *In vivo* mean stresses in the axial and circumferential directions were not restored suggesting that stress, while a target for growth and remodeling in cases of altered loading conditions,[17,19,23] may not be the primary target in development and maturation. Indeed, these results suggest that cyclic strain is restored during maturation, with *in vivo* stresses, perhaps being a secondary target for growth and remodeling. This speculation, however, warrants further investigation as other reports in the literature may suggest otherwise.[23]

There are several limitations to the current approach. First, although we seek to identify the role of a single extracellular matrix protein (fibulin-5) on the overall biomechanical behavior of arteries, interpretation of these data is complicated by the fact that, throughout their development and maturation, mechanisms could compensate for the lack of fibulin-5. Nevertheless, given the striking differences in the mechanical and microstructural behavior of *fbln5*$^{-/-}$ vs. *fbln5*$^{+/+}$, broad conclusion regarding the role of functional elastin fiber may be made. Second, we present plots of mean stress vs. mid-wall strain and perform stress analyses with the assumption that the tissue is homogeneous. Clearly, however, there are significant heterogeneities, particularly between the media and adventitia, in mouse CCAs.

Future studies could include the incorporation of such heterogeneities, which may be based on heterogeneities in the content and organization of cells and extracellular matrix observed in our stacks of confocal microscopy images. Third, although the constitutive model employed here is microstructurally motivated, no direct correlations are made between material parameters and cell and extracellular matrix content and organization. Thus, future studies may include the use of constrained mixture models to ascribe such microstructural meaning to each parameter.[12]

In summary, biaxial mechanical tests have revealed distinct differences in the material properties of the $fbln5^{+/+}$ and $fbln5^{-/-}$ arteries while confocal and multiphoton imaging have revealed structural differences in elastin, collagen and smooth muscle cell organization between $fbln5^{+/+}$ and $fbln5^{-/-}$ arteries. Analysis of the $fbln5^{-/-}$ mouse suggests that elastin plays a key role in the mechanical response of mouse carotid arteries and that functional elastic fibers appear to be necessary for the normal development of the *in vivo* axial stretch ratio. Further studies that quantify the microstructure and constitutive modeling with more advanced models will provide a more definitive link between the microstructure and mechanics of $fbln5^{-/-}$ arteries.

## Acknowledgments

We gratefully acknowledge that this research was funded by grants from the NIH (R21-HL085822 and T32-GM008433).

## References

1. Arnet DK, Evans GW, Riley WA. Arterial stiffness: a new cardiovascular risk factor? Am J Epidemiol. 1994; 140:669–682. [PubMed: 7942769]
2. Baek S, Gleason R, Rajagopal K, Humphrey J. Theory of small on large: potential utility in computations of fluid–solid interactions in arteries. Comput Methods Appl Mech Eng. 2007; 196(31–32):3070–3078.
3. Chuong CJ, Fung YC. On residual stresses in arteries. J Biomech Eng. 1986; 108(2):189–192. [PubMed: 3079517]
4. Davies PF. Flow-mediated endothelial mechanotransduction. Physiol Rev. 1995; 75(3):519–560. [PubMed: 7624393]
5. Dobrin PB. Biaxial anisotropy of dog carotid artery: estimation of circumferential elastic modulus. J Biomech. 1986; 19(5):351–358. [PubMed: 3733760]
6. Dye WW, Gleason RL, Wilson E, Humphrey JD. Altered biomechanical properties of carotid arteries in two mouse models of muscular dystrophy. J Appl Physiol. 2007; 103(2):664–672. [PubMed: 17525297]
7. Dzau VJ, Gibbons GH. Vascular remodeling: mechanisms and implications. J Cardiovasc Pharmacol. 1993; 21(Suppl 1):S1–S5. [PubMed: 7681124]
8. Eberth JF, Taucer AI, Wilson E, Humphrey JD. Mechanics of carotid arteries in a mouse model of Marfan Syndrome. Ann Biomed Eng. 2009; 37(6):1093–1104. [PubMed: 19350391]
9. Fillinger MF, Racusin J, Baker RK, Cronenwett JL, Teutelink A, Schermerhorn ML, Zwolak RM, Powell RJ, Walsh DB, Rzucidlo EM. Anatomic characteristics of ruptured abdominal aortic aneurysm on conventional CT scans: implications for rupture risk. J Vasc Surg. 2004; 39(6):1243–1252. [PubMed: 15192565]
10. Fung, Y. Biomechanics: Mechanical Properties of Living Tissues. Springer; 1993.
11. Gleason RL, Gray SP, Wilson E, Humphrey JD. A multiaxial computer-controlled organ culture and biomechanical device for mouse carotid arteries. J Biomech Eng. 2004; 126(6):787–795. [PubMed: 15796337]
12. Hansen L, Wan W, Gleason RL. Microstructurally-motivated constitutive modeling of mouse arteries cultured under altered axial stretch. J Biomech Eng. 2009; 131(10):11.

13. Holzapfel GA, Gasser TC, Ogden RW. A new constitutive framework for arterial wall mechanics and a comparative study ofmaterialmodels. J Elast. 2000; 61:1–48.
14. Holzapfel G, Gasser T, Ogden R. Comparison of a multi-layer structural model for arterial walls with a fung-type model, and issues of material stability. J Biomech Eng. 2004; 126(2):264. [PubMed: 15179858]
15. Humphrey, JD. Cardiovascular Solid Mechanics: Cells, Tissues, Organs. New York: Springer-Verlag; 2002.
16. Humphrey JD, Rajagopal KR. A constrained mixture model for growth and remodeling of soft tissues. Math Models Methods Appl Sci. 2002; 12(3):407–430.
17. Jackson ZS, Dajnowiec D, Gotlieb AI, Langille BL. Partial off-loading of longitudinal tension induces arterial tortuosity. Arterioscler Thromb Vasc Biol. 2005; 25(5):957–962. [PubMed: 15746437]
18. Jackson ZS, Gotlieb AI, Langille BL. Wall tissue remodeling regulates longitudinal tension in arteries. Circ Res. 2002; 90(8):918–925. [PubMed: 11988494]
19. Kamiya A, Togawa T. Adaptive regulation of wall shear stress to flow change in the canine carotid artery. Am J Physiol. 1980; 239(1):H14–H21. [PubMed: 7396013]
20. Kobayashi N, Kostka G, Garbe JH, Keene DR, Bachinger HP, Hanisch FG, Markova D, Tsuda T, Timpl R, Chu ML, Sasaki T. A comparative analysis of the fibulin protein family. Biochemical characterization, binding interactions, and tissue localization. J Biol Chem. 2007; 282(16):11805–11816. [PubMed: 17324935]
21. Kowal RC, Richardson JA, Miano JM, Olson EN. EVEC, a novel epidermal growth factor-like repeat-containing protein upregulated in embryonic and diseased adult vasculature. Circ Res. 1999; 84:1166–1176. [PubMed: 10347091]
22. Martinez-Lemus LA, Hill MA, Bolz SS, Pohl U, Meininger GA. Acute mechanoadaptation of vascular smooth muscle cells in response to continuous arteriolar vasoconstriction: implications for functional remodeling. FASEB J. 2004; 18(6):708–710. [PubMed: 14977879]
23. Matsumoto T, Hayashi K. Stress and strain distribution in hypertensive and normotensive rat aorta considering residual strain. J Biomech Eng. 1996; 118(1):62–73. [PubMed: 8833076]
24. Nakamura T, Lozano PR, Ikeda Y, Iwanaga Y, Hinek A, Minamisawa S, Cheng CF, Kobuke K, Dalton N, Takada Y, Tashiro K, Ross J Jr, Honjo T, Chien KR. Fibulin-5/DANCE is essential for elastogenesis in vivo. Nature. 2002; 415(6868):171–175. [PubMed: 11805835]
25. Roach MR, Burton AC. The reason for the shape of the distensibility curves of arteries. Can J Biochem Physiol. 1957; 35(8):681–690. [PubMed: 13460788]
26. Spencer, AJM. Constitutive theory for strongly anisotropic solids. Continuum Theory of the Mechanics of Fibre-Reinforced Composites, CISM Courses and Lectures No. 282. In: Spencer, AJM., editor. International Centre for Mechanical Sciences. Springer-Verlag; Wien: 1984. p. 1-32.
27. Takamizawa K, Hayashi K. Strain energy density function and uniform strain hypothesis for arterial mechanics. J Biomech. 1987; 20(1):7. [PubMed: 3558431]
28. Van Loon P. Length–force and volume–pressure relationships of arteries. Biorheology. 1977; 14(4):181–201. [PubMed: 912047]
29. Wagenseil JE, Ciliberto CH, Knutsen RH, Levy MA, Kovacs A, Mecham RP. Reduced vessel elasticity alters cardiovascular structure and function in newborn mice. Circ Res. 2009; 104(10): 1217–1224. [PubMed: 19372465]
30. Wagenseil JE, Nerurkar NL, Knutsen RH, Okamoto RJ, Li DY, Mecham RP. Effects of elastin haploinsufficiency on the mechanical behavior of mouse arteries. Am J Physiol Heart Circ Physiol. 2005; 289(3):H1209–H1217. [PubMed: 15863465]
31. Wong LC, Langille BL. Developmental remodeling of the internal elastic lamina of rabbit arteries: effect of blood flow. Circ Res. 1996; 78(5):799–805. [PubMed: 8620599]
32. Yanagisawa H, Davis EC, Starcher BC, Ouchi T, Yanagisawa M, Richardson JA, Olson EN. Fibulin-5 is an elastin-binding protein essential for elastic fibre development in vivo. Nature. 2002; 415(6868):168–171. [PubMed: 11805834]
33. Zoumi A, Yeh A, Tromberg BJ. Imaging cells and extracellular matrix in vivo by using second-harmonic generation and two-photon excited fluorescence. Proc Natl Acad Sci USA. 2002; 99(17): 11014–11019. [PubMed: 12177437]

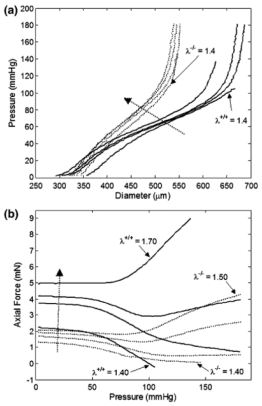


**FIGURE 1.**

Representative plots of pressure–diameter (a) and pressure–force (b) results for *fbln5* $^{+/+}$ (solid lines) and *fbln5* $^{-/-}$ (dotted lines) arteries. Curves for the *fbln5* $^{-/-}$ plot indicate axial stretch ratios of $\lambda = 1.40$, $\lambda = 1.45$, $\lambda = 1.48$, and $\lambda = 1.50$, while curves for the *fbln5* $^{+/+}$ plot indicate axial stretch ratios of $\lambda = 1.40$, $\lambda = 1.60$, $\lambda = 1.65$, and $\lambda = 1.70$. Dotted arrow indicates direction of increasing axial stretch ratios. The exponentially stiffening portion of the mechanical response of *P–d* curves occurs at smaller diameters in *fbln5* $^{-/-}$ arteries.

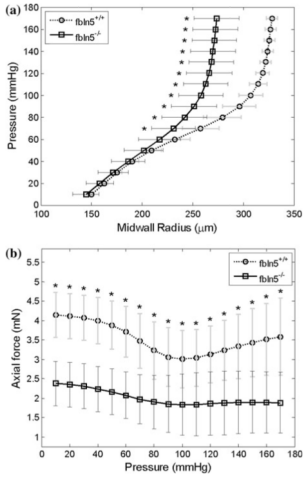


**FIGURE 2.**

Mean pressure-mid-wall radii (a) and pressure–force (b) plots for *fbln5* $^{+/+}$ (circles) and *fbln5*$^{-/-}$ (squares) arteries. Data were collected at the *in vivo* axial stretch ratio and indicate that *fbln5* $^{-/-}$ vessels had smaller circumferential dimensions. Asterisks indicate $p<0.05$; error bars indicate standard deviation.

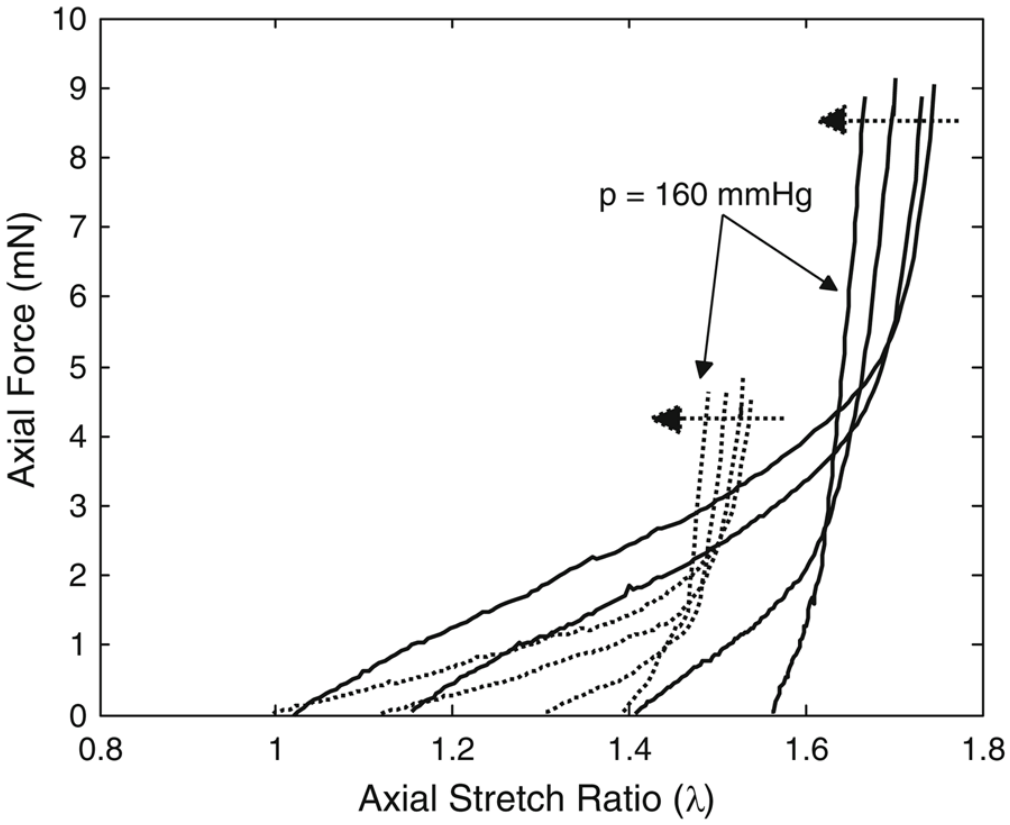


**FIGURE 3.**

Representative plots of axial force-stretch results for *fbln5* $^{+/+}$ (solid lines) and *fbln5* $^{-/-}$ (dotted lines) arteries. Axial force-stretch tests were conducted at pressures of $P = 0$, $P = 60$, $P = 100$, and $P = 160$ mmHg. Dotted arrows indicate direction of increasing pressure. The crossover points represent *in vivo* axial stretch ratios; and the data suggest that *fbln5* $^{-/-}$ vessels have a lower *in vivo* axial stretch ratio.

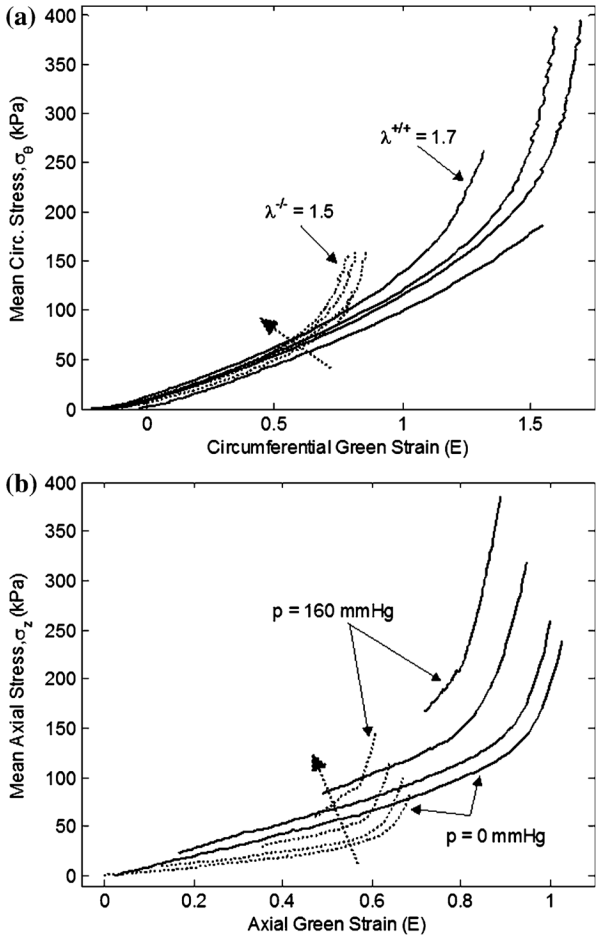


**FIGURE 4.**

Representative plots of mean circumferential stress–strain (a) and mean axial stress–strain (b) results for *fbln5* $^{+/+}$ (solid lines) and *fbln5* $^{-/-}$ (dotted lines) arteries. For the circumferential stress–strain plot, curves for the *fbln5* $^{-/-}$ plot indicate axial stretch ratios of $\lambda = 1.40$, $\lambda = 1.45$, $\lambda = 1.48$, and $\lambda = 1.50$, while curves for the *fbln5* $^{+/+}$ plot indicate axial stretch ratios of $\lambda = 1.40$, $\lambda = 1.60$, $\lambda = 1.65$, and $\lambda = 1.70$. For the axial stress–strain plot, curves reflect tests conducted at pressures of $P = 0$, $P = 60$, $P = 100$, and $P = 160$ mmHg. Dotted arrows reflect the direction of increasing axial stretch ratio or direction of increasing pressure. The exponentially stiffening portion of the curves occurs at lower strains in the *fbln5* $^{-/-}$ artery.

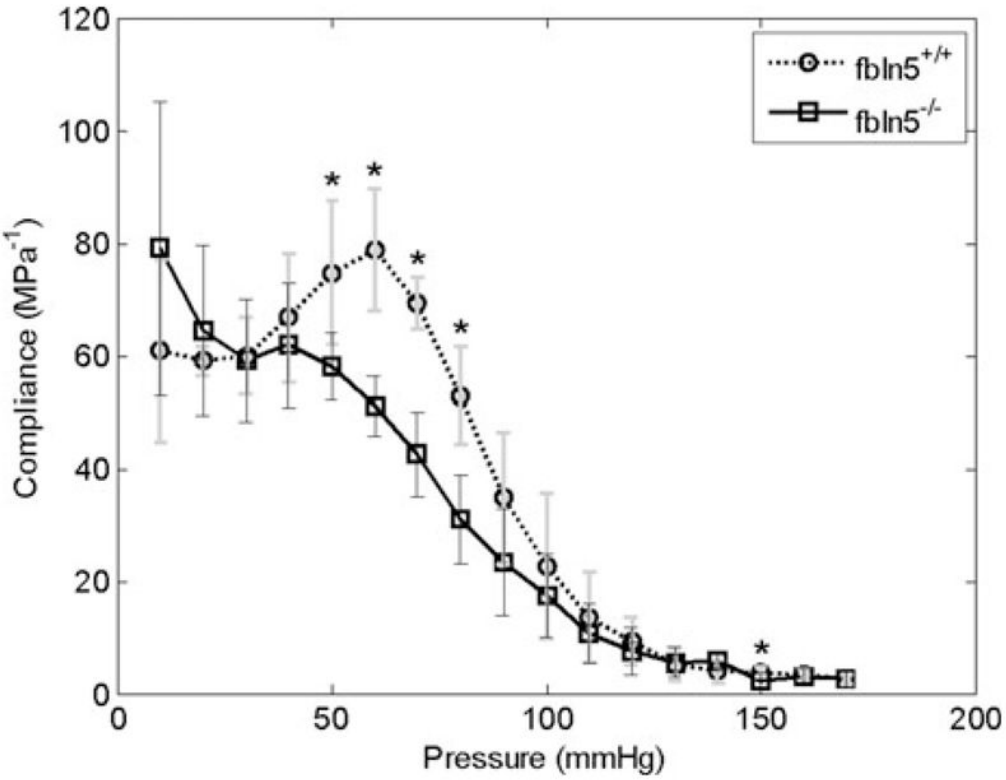


**FIGURE 5.**

Compliance calculated at 10 mmHg intervals at the *in vivo* axial stretch ratio. At overlapping physiological pressures, there were no significant differences in compliance. Asterisks indicate $p < 0.05$; errors bars indicate one standard deviation.

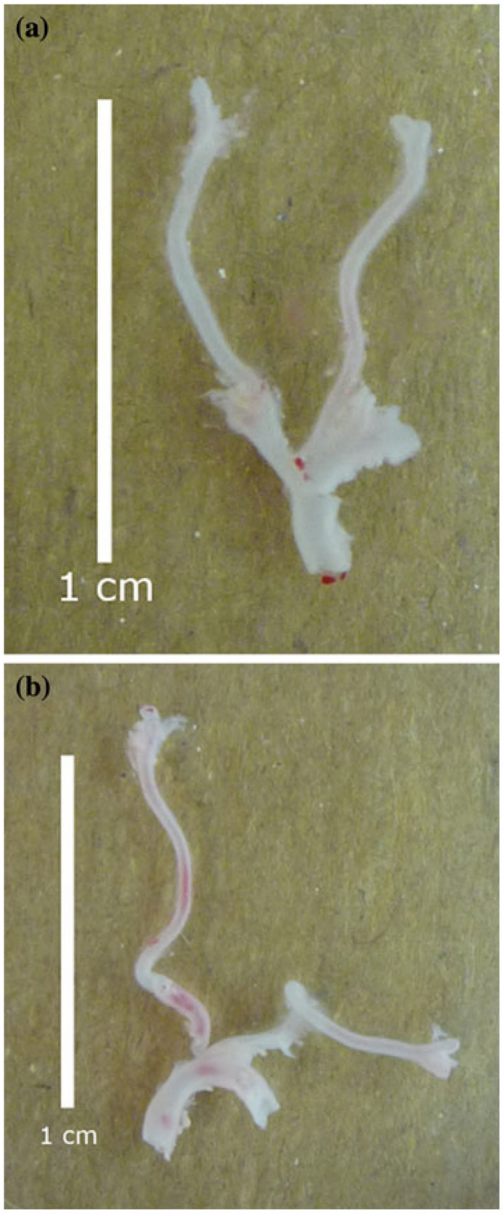


**FIGURE 6.**

Representative images of excised arteries from *fbln5* $^{+/+}$ (a) and *fbln5* $^{-/-}$ (b) vessels. Vessels in the unloaded state from knockout mice exhibit significant tortuosity compared with slight bending observed in wild-type vessels.

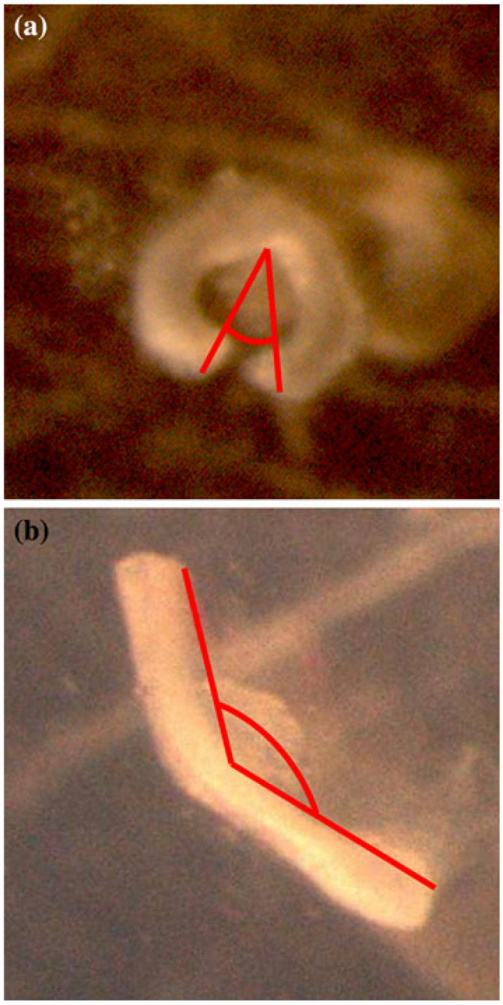


**FIGURE 7.**
Representative opening angle sectors from *fbln5* $^{+/+}$ (a) and *fbln5* $^{-/-}$ (b) arteries.

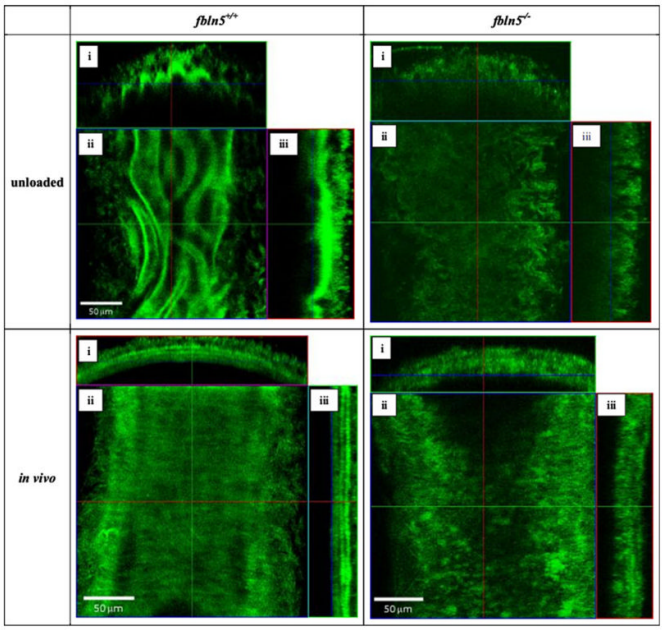


**FIGURE 8.**

The undulated internal elastic lamina is clearly visible in the traction-free configuration of the *fbln5* $^{+/+}$ artery while elastin is more disorganized in the *fbln5* $^{-/-}$ artery. When pressurized to *in vivo* conditions, elastin is organized into lamellar units and is visible in the *fbln5* $^{+/+}$ artery while in the *fbln5* $^{-/-}$ artery, elastin remains disorganized. Panels i, ii, and iii show cross, *en face*, and longitudinal sections, respectively.

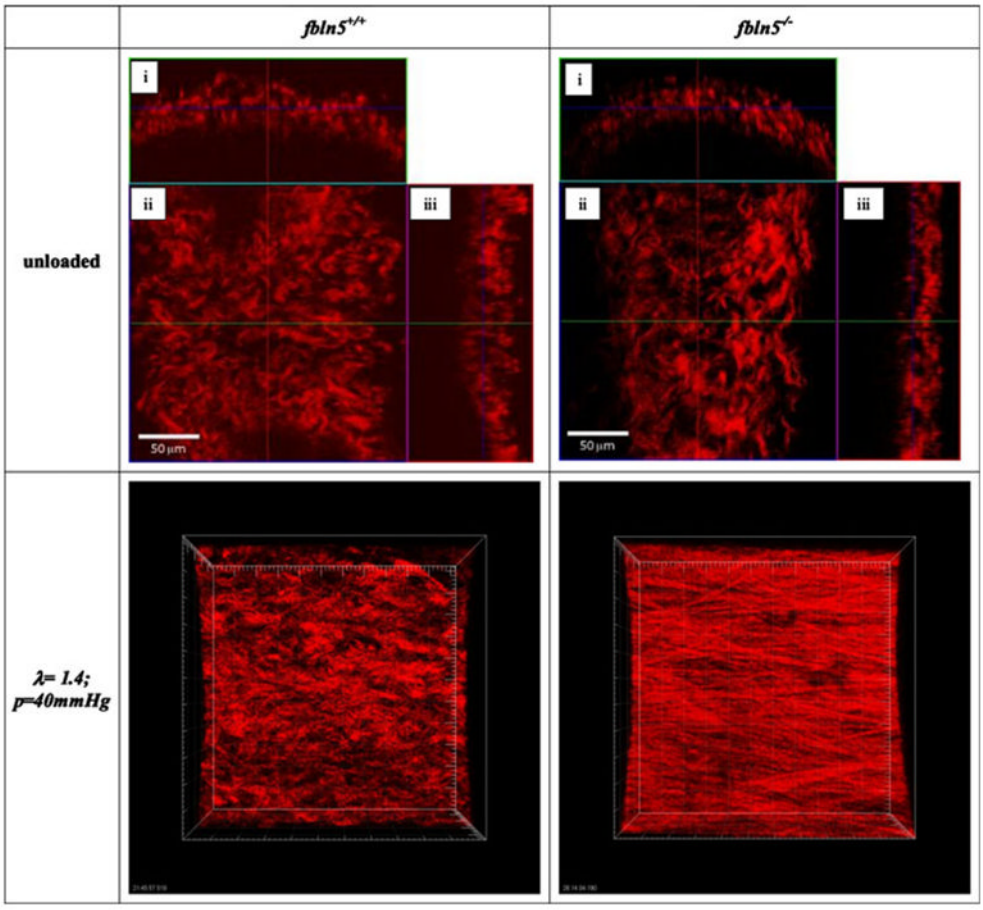


**FIGURE 9.**

In the traction-free state, collagen fibers in the *fbln5* $^{+/+}$ artery and the *fbln5* $^{-/-}$ artery have different degrees of undulation. Panels i, ii, and iii show cross, *en face*, and longitudinal sections, respectively. Collagen was imaged at an axial stretch of $\lambda = 1.4$ and transmural pressure of $P = 40$ mmHg for both knockout and wild-type arteries; images were stacked to generate a 3D reconstruction (axis of the vessel oriented horizontally). Collagen fibers from the *fbln5* $^{-/-}$ vessel appear straightened while collagen fibers from the *fbln5* $^{+/+}$ vessel appear undulated, indicating that collagen fibers in *fbln5* $^{-/-}$ vessels become engaged at a lower axial stretch ratio.

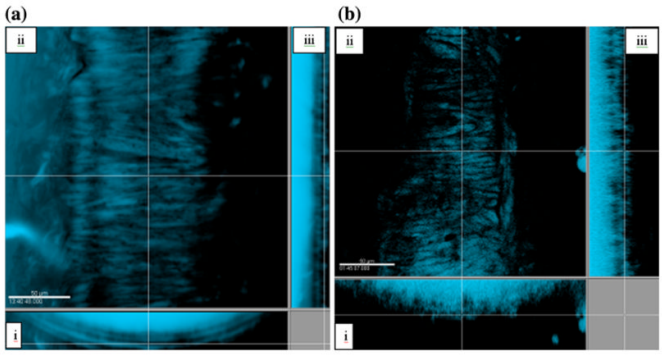


**FIGURE 10.**

SMC from the *fbln5* $^{+/+}$ artery (a) are arranged into lamellar units while SMC from the *fbln5* $^{-/-}$ artery (b) lack lamellar structure. Panels i, ii, and iii show cross, *en face*, and longitudinal sections, respectively.

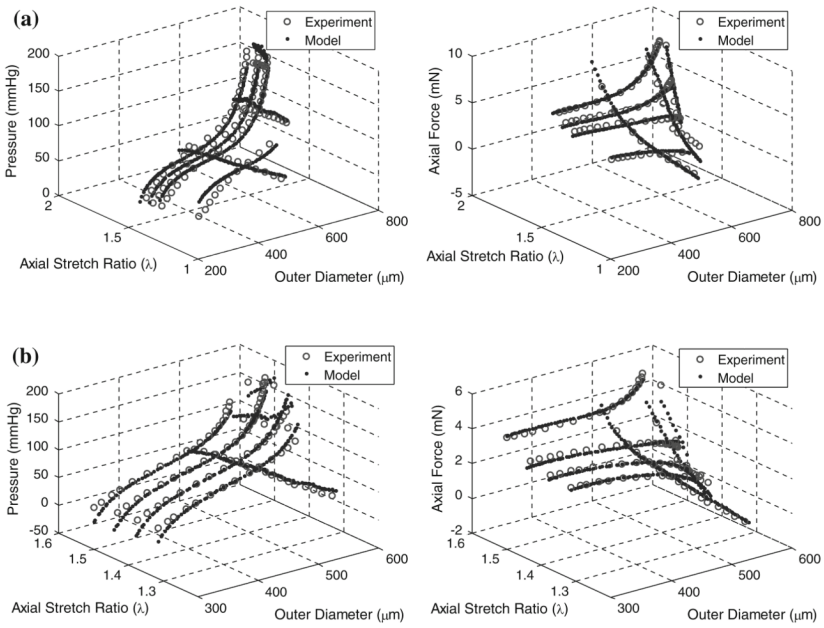


**FIGURE 11.**

Illustrative plots of pressure and axial force vs. diameter and axial stretch ratio for model predictions (filled circle) and experimentally measured (open circle) for *fbln5* $^{+/+}$ (a) and *fbln5* $^{-/-}$ (b) arteries. At lower diameters, these two cases show the model overestimating pressure for the *fbln5* $^{+/+}$ artery while underestimating pressure for the *fbln5* $^{-/-}$ artery.

## TABLE 1

Animal age and weight and vessel geometry, contractile response, and mechanical metrics for *fbln5* $^{+/+}$ and *fbln5* $^{-/-}$ mice.

| | ***fbln5*$^{+/+}$ (*n* = 6)** | ***fbln5*$^{-/-}$ (*n* = 7)** |
|---|---|---|
| Age (weeks) | 13 (1) | 13 (5) |
| Body weight (g) | 28.93 (1.88) | 24.04 (2.65)* |
| Opening angle | 86.6 (14.1) | 150 (12)* |
| Unloaded dimensions ($\mu$m) | | |
| Inner diameter | 248 (34) | 202 (99) |
| Outer diameter | 403 (21) | 417 (23) |
| Wall thickness | 77.1 (15.3) | 108 (42) |
| *In vivo* dimensions ($\mu$m) | | |
| Inner diameter | 603 (25) | 492 (57)* |
| Outer diameter | 652 (23) | 577 (43)* |
| Wall thickness | 24.3 (4.5) | 42.6 (11.1)* |
| *In vivo* axial stretch ratio | 1.64 (0.03) | 1.41 (0.07)* |
| Maximal contraction (%) | 12.6 (6.0) | 4.60 (2.88)* |
| Physiological compliance ($MPa^{-1}$) | 14.0 (7.4) | 8.51 (3.62) |
| Linearized cyclic strain (%) | 7.76 (4.13) | 6.46 (2.75) |
| Mean *in vivo* stresses (kPa) | | |
| Circumferential | 194 (38) | 101 (32)* |
| Axial | 159 (29) | 74.4 (27.9)* |

Values are means (SD).

Asterisks indicate statistical significant differences (* $p<0.05$).

**TABLE 2**

Material parameters for *fbln5* $^{+/+}$ and *fbln5* $^{-/-}$ CCAs obtained for a four-fiber constitutive model.

| | ***b*** **(kPa)** | $b_1^1$ (kPa) | $b_2^1$ | $b_1^2$ (kPa) | $b_2^2$ | $b_1^3$ (kPa) | $b_2^3$ | ***α*** | **Error** |
|---|---|---|---|---|---|---|---|---|---|
| *fbln5* $^{+/+}$ | | | | | | | | | |
| 1 | 26.295 | 0.036 | 0.709 | 0.141 | 1.201 | 0.576 | 0.835 | 43.1 | 0.104 |
| 2 | 26.905 | 3.569 | 0.129 | 0.611 | 0.768 | 0.803 | 0.885 | 32.9 | 0.060 |
| 3 | 17.004 | 0.431 | 0.216 | 0.418 | 0.783 | 0.246 | 0.850 | 32.0 | 0.033 |
| 4 | 40.516 | 0.974 | 0.278 | 0.105 | 0.932 | 0.012 | 1.562 | 41.2 | 0.055 |
| 5 | 31.285 | 0.385 | 0.290 | 0.333 | 1.004 | 0.370 | 0.861 | 33.6 | 0.071 |
| 6 | 13.805 | 3.153 | 0.044 | 17.744 | 0.000 | 0.274 | 0.726 | 30.7 | 0.024 |
| Mean | 25.968 | 1.425 | 0.278 | 3.225 | 0.781* | 0.380 | 0.953* | 35.6 | 0.058 |
| SD | 9.687 | 1.535 | 0.231 | 7.115 | 0.415 | 0.276 | 0.303 | 5.2 | 0.029 |
| *fbln5* $^{-/-}$ | | | | | | | | | |
| 1 | 26.735 | 5.077 | 0.859 | 0.000 | 5.537 | 0.050 | 3.426 | 36.1 | 0.033 |
| 2 | 24.002 | 2.940 | 0.633 | 0.610 | 2.659 | 1.080 | 2.026 | 40.7 | 0.025 |
| 3 | 26.699 | 0.963 | 0.625 | 0.032 | 5.305 | 0.368 | 2.688 | 34.9 | 0.051 |
| 4 | 0.189 | 0.727 | 0.068 | 4.876 | 1.078 | 2.682 | 0.399 | 36.5 | 0.070 |
| 5 | 0.133 | 2.313 | 0.023 | 9.448 | 0.000 | 1.688 | 0.717 | 25.9 | 0.054 |
| 6 | 11.716 | 0.992 | 0.353 | 0.990 | 5.638 | 0.447 | 3.450 | 29.9 | 0.017 |
| 7 | 19.889 | 6.527 | 0.306 | 0.000 | 9.086 | 0.081 | 3.139 | 34.4 | 0.041 |
| Mean | 15.623 | 2.791 | 0.410 | 2.279 | 4.186* | 0.914 | 2.264* | 34.1 | 0.042 |
| SD | 11.747 | 2.246 | 0.310 | 3.606 | 3.128 | 0.975 | 1.267 | 4.8 | 0.018 |

Values are means (SD).

Asterisks indicate that the parameter is statistically different between knockout and wild-type mice (* $p<0.05$).

*Ann Biomed Eng*. Author manuscript; available in PMC 2011 May 19.